PHILOSOPHICAL TRANSACTIONS OF THE ROYAL SOCIETY A MATHEMATICAL, PHYSICAL & ENGINEERING SCIENCES

Temperature and Composition Measurements from the l.r.i.r. and l.i.m.s. Experiments on Nimbus 6 and 7

J. C. Gille, P. L. Bailey and J. M. Russell

Phil. Trans. R. Soc. Lond. A 1980 **296**, 205-218
doi: 10.1098/rsta.1980.0165

Phil. Trans. R. Soc. Lond. A **296**, 205–218 (1980) [205]
Printed in Great Britain

Temperature and composition measurements from the l.r.i.r. and l.i.m.s. experiments on Nimbus 6 and 7

By J. C. Gille,† P. L. Bailey† and J. M. Russell III‡§

† *National Center for Atmospheric Research, Boulder, Colorado* 80307, *U.S.A.*
‡ *N.A.S.A. Langley Research Center, National Aeronautics and Space Administration, Hampton, Virginia* 23665, *U.S.A.*

The limb radiance inversion radiometer (l.r.i.r.) on Nimbus 6 was the first orbiting infrared limb scanner. It had four channels with which to determine temperature, O_3 and H_2O in the stratosphere and low mesosphere. The limb infrared monitor of the stratosphere (l.i.m.s.) is a similar six-channel instrument launched on Nimbus 7 in October 1978 to measure temperature, O_3, H_2O, NO_2 and HNO_3. The instrumentation and inversion techniques are briefly described. In this method, the outwelling radiance in the 15 μm bands of CO_2 is inverted to yield temperatures as a function of pressure; the temperature is then used with the radiance emitted by a trace gas to determine its concentration. L.r.i.r. temperature and ozone results show high precision and good agreement with rocket measurements from the tropopause into the mesosphere. Preliminary l.i.m.s. results show that temperatures may be retrieved into the troposphere, and the capability to determine constituent concentrations in the part/10^9 range from a satellite for the first time.

The application of such data for photochemical, dynamical and transport problems is discussed.

1. Introduction

Understanding the many processes – radiative, chemical and dynamical – that take place in the middle atmosphere requires global observations not only of temperature but also composition. The retrieval of temperature and composition information from measurements of infrared radiation emitted by the atmosphere, observed as a function of position on the Earth's limb, has advantages over other techniques for obtaining these data.

The limb radiance inversion radiometer (l.r.i.r.) on Nimbus 6 was the first satellite-borne limb scanner. It obtained its measurements in four channels, in order to infer the vertical distribution of temperature (T), ozone (O_3), and water vapour (H_2O). Subsequently, the limb infrared monitor of the stratosphere (l.i.m.s.) instrument was developed for flight on Nimbus 7. It is similar to the l.r.i.r., but incorporates additional channels for the measurement of nitrogen dioxide (NO_2) and nitric acid (HNO_3), as well as changing the H_2O channel and other improvements.

In this paper we shall review the instrumentation and principles of these limb scanners, present examples of the results, and discuss the applications of the data.

The features of limb scanning, discussed by Gille & House (1971, hereafter referred to as G.H.), follow from the geometry. The atmospheric emission stands out against cold space, and does not require the removal of a background signal. It is enhanced by the large amount

§ Associated only with l.i.m.s. experiment.

of emitting material in the long tangential paths through the atmosphere. Both of these features are very useful for determining the distribution of trace species. The measurement of emission, of course, allows measurements at all local times and latitudes which may be viewed from the spacecraft.

Another feature is the inherent potential for high vertical resolution. The path through a shell 1 km thick at the tangent point is nearly 4.5 times longer than that through the shell 1 km higher. (Thereafter, the geometric path decreases more slowly, and the decrease of opacity is generally dominated by the decrease of constituent concentration with altitude.)

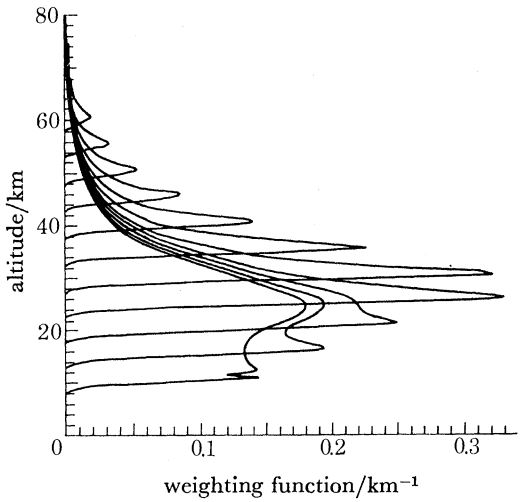

FIGURE 1. Representative weighting functions for the l.r.i.r. wide 15 μm CO_2 channel (WCO_2) used for temperature retrievals. These were calculated by convolving infinitesimal weighting functions (Gille & House 1971) with a nominal 2 km field of view. Actual weighting functions were spaced every 1.5 km in the vertical.

The altitude distributions of opacity or weighting functions (see below) for an optically thin ray path through the atmosphere have half-power points which are about 3 km apart in altitude, roughly a quarter of the width of weighting functions for downward viewing. These, of course, must be convolved with a finite field of view for a real instrument. The instruments described here have employed narrow fields of view in order to take advantage of this capability. A set of representative weighting functions for temperature sounding are shown in figure 1. Note that their vertical spacing depends upon scan rate and sampling frequency, while the width and shape depend upon field of view and atmospheric transmission. One may use broader fields of view, but generally at the expense of achievable vertical resolution.

Two radiance profiles from l.r.i.r. are illustrated in figure 2. In both cases, the emission increases from small values at high altitudes, where the atmospheric paths are nearly transparent, to large values at low altitudes. The narrow CO_2 channel, in the centre of the 15 μm bands, is an example of a band that becomes opaque in the stratosphere, and for which the signals are Planck black body radiances of typical stratospheric temperatures. The radiance variations are due only to atmospheric temperature variations.

The ozone channel radiance is representative of the case in which the gaseous constituent is not opaque, but allows clouds in the upper troposphere to be seen. These give large and

variable signals (black body radiances at tropospheric temperatures), but also allow some cloud height information to be derived. Whether from the gas or cloud, the large opacities at low altitudes put a lower limit on the region that may be sounded. The noise level, which determines how small a signal may be measured with useful precision, controls the upper limit of coverage. For the experiments described here, useful information has been achieved from the upper troposphere (*ca.* 11–70 km).

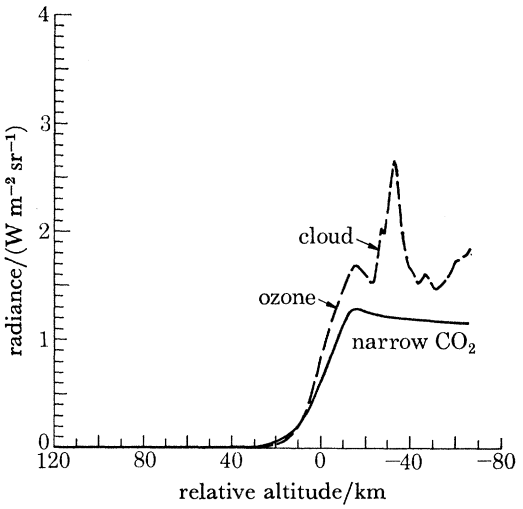

FIGURE 2. Radiance profiles in two l.r.i.r. channels. Solid line: narrow 15 μm CO channel (NCO_2). Dashed line: ozone channel.

It is also pointed out in figure 2 that radiances are measured as a function of angle, or relative altitude. It is necessary to determine the pressure (or density) for the lowest point along a ray path from the data themselves, as noted below, and thereby to obtain an absolute altitude.

In the following, § 2 contains a review of the instrumentation. The inversion of the radiance data is outlined in § 3, and some results are presented in § 4. Examples of applications of the data are given in § 5.

2. THE L.R.I.R. AND L.I.M.S. INSTRUMENTS

The optical schematic of the l.r.i.r. and l.i.m.s. is shown in figure 3.

Radiance from the Earth's limb comes through a hood and baffle assembly to the scan mirror, which directs the beam to an 18 cm off-axis parabolic primary. The radiation is chopped (940 Hz) at the focus of the primary, re-collected and directed into the detector capsule assembly.

Here the radiation passes through a series of optical elements which focus the beam through interference filters, a field of view defining mask, and on to an array of mercury–cadmium–telluride detectors.

The train from the Irtran-6 lens back to the detectors is maintained at 63 K by a cold finger from a block of solid methane, which serves as the primary cryogen. Its life is extended by a thermal shield maintained at 152 K by the solid ammonia secondary cryogen. This also

maintains the temperature of the optical train from the thermal mask through the parabolas at 152 K. The ammonia and methane are contained in the solid cryogen dewar. The life of the experiment is limited by the 6.2 kg mass of methane to about 7 months.

In operation, a servo-controlled motor drives the scan mirror, so that the fields of view cross the infrared limb from above 100 km to below the hard surface at a constant rate ($1^\circ\ s^{-1}$ for l.r.i.r., $0.25^\circ\ s^{-1}$ for l.i.m.s.). The precise relative angular position is determined from the output of an encoder on the mirror shaft, which puts out a pulse every 40 ± 2 arcsec.

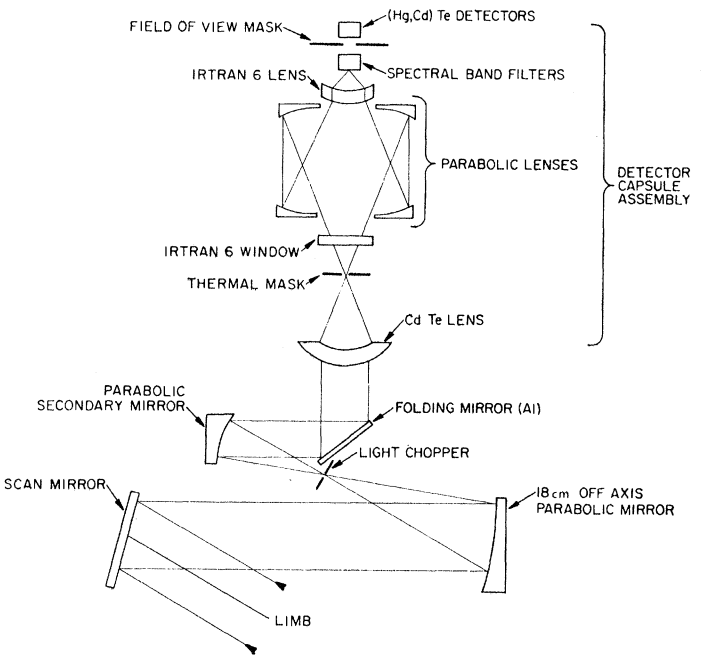

FIGURE 3. Optical schematic diagram of the l.r.i.r. and l.i.m.s.

TABLE 1. CHARACTERISTICS OF L.R.I.R. CHANNELS

channel	purpose	band/pass 50 % relative response points/cm^{-1}	field-of-view at limb/km		noise equivalent radiance/($W\ m^{-2}\ sr^{-1}$)
			vertical	horizontal	
1	NCO_2	649–672	2.0	20	0.0023
2	WCO_2	592–700	2.0	20	0.0040
3	O_3	984–1169	2.0	20	0.011
4	H_2O	412–446	2.5	25	0.008

TABLE 2. CHARACTERISTICS OF L.I.M.S. CHANNELS

channel	purpose	bandpass 50 % relative response points/cm^{-1}	field-of-view at limb/km		noise equivalent radiance/($W\ m^{-2}\ sr^{-1}$)
			vertical	horizontal	
1	NO_2	1580–1613	3.6	28	0.0006
2	H_2O	1396–1527	3.6	28	0.0021
3	O_3	947–1103	1.8	18	0.0035
4	HNO_3	859–900	1.8	18	0.0015
5	WCO_2	595–739	1.8	18	0.005
6	NCO_2	645–673	1.8	18	0.0013

The l.r.i.r. channel characteristics are displayed in table 1. The radiometer channel outputs were sampled on the encoder pulses, at a nominal sample interval of 22 ms. The data were read out in 12 bit words. In-flight calibration occurred every 32 s.

The l.i.m.s. channels are described in table 2. The major difference, apart from the additional channels and slower scan, is the clock initiated data sampling every 24 ms. A number of improvements and lesser changes were also incorporated. In-flight calibration occurs every 28 s.

The l.r.i.r. and l.i.m.s. experiments have been discussed in greater detail by, respectively, Gille *et al.* (1975) and Russell & Gille (1978).

3. Inversion of radiance profiles

The equation for the emerging radiance I within a spectral band may be written

$$I(h) = \int_{-\infty}^{\infty} B(x) \frac{\mathrm{d}\tau(h, x)}{\mathrm{d}x} \mathrm{d}x, \tag{1}$$

where h is the tangent height of the ray path, B is the Planck black body function for the band, $\tau(h, x)$ is the transmittance from the point x to the spacecraft along the ray path having tangent height h, and x is the coordinate along the ray path.

The general approach is to measure the outgoing radiance from carbon dioxide (CO_2), whose distribution is known, and for which the terms $\mathrm{d}\tau/\mathrm{d}x$ may be calculated. From these, B and, thus the temperature, are determined. For other gases, B is calculated for the appropriate band from the temperature, and used with the measured I to determine $\mathrm{d}\tau/\mathrm{d}x$ from which the required trace gas concentrations may be obtained.

A major problem as noted above is that the Nimbus attitude control and ephemeris data do not allow h for a given measurement to be determined very well. Even if this were possible it would not be enough, since it is necessary to know the absorber density at h, which is controlled by the temperature structure through the hydrostatic equation. The solution was developed in G.H.

After converting (1) to a vertical integral,

$$I(h) = \int_{h}^{\infty} B(z) \left[\left(\frac{\mathrm{d}\tau(h, z)}{\mathrm{d}x} \right)_{\mathrm{a}} + \left(\frac{\mathrm{d}\tau(h, z)}{\mathrm{d}x} \right)_{\mathrm{p}} \right] \left| \frac{\mathrm{d}x}{\mathrm{d}z} \right| \mathrm{d}z, \tag{2}$$

(where subscripts a, p refer to points on the path anterior and posterior to the tangent point), equation (2) may be written

$$I(h - z_0) = p_0 R^{-1} C_1 \int_{h - z_0}^{\infty} B(z)\, L(h, z) \left| \frac{\mathrm{d}x}{\mathrm{d}z} \right|_z \times \exp\left[-\int_{z_0}^{z} g R^{-1} T(z')^{-1} \mathrm{d}z' \right] T(z)^{-1} \mathrm{d}z = p_0 \int_{h - z_0}^{\infty} B(z)\, W(h, z) \mathrm{d}z, \tag{3}$$

where $L(h, z)$ contains the derivatives of the transmittance in terms of absorber amount and pressure along the path, C_1 represents the mixing ratio of CO_2, and $p_0 W$ is the weighting function mentioned above. The only reference point needed is an arbitrary level z_0, corresponding to one of the radiance samples at which the pressure is p_0. G.H. then showed that p_0 could be determined from measurements in two CO_2 channels for which the atmosphere has different opacities.

The iterative procedure described there is too slow for operational use, as well as leading to error growth when a large number of iterations is used. It has been necessary to develop a fast but accurate method for performing the retrievals. The procedure now in use (Bailey & Gille 1978) begins with a pre-inversion stage, in which an up and a down profile (taken within 4 s, or 25 km, of ground track for l.r.i.r.) are used to determine the mean spacecraft motion, then combined into a single profile and the cloud tops located from radiances in a non-opaque channel such as the ozone channel.

The data are then Fourier transformed into a spatial frequency domain, low pass filtered for noise suppression and 'boosted' to partially compensate the effects of the finite field of view (Gille & Bailey 1978) before being transformed back into physical space.

Inversion then takes place in two steps. In an initial or direct inversion (Bailey & Gille 1978), (3) is written as

$$I(p) = B[\hat{T}]\, \epsilon(p, \hat{T}), \tag{4}$$

where p is the pressure at the tangent point, $\hat{T}$ is an average temperature over the region of the atmosphere contributing to the outgoing radiance, defined by

$$\hat{T} = \int_h^H W(h, z)\, T(z)\, \mathrm{d}z \Big/ \int_h^H W(h, z)\, \mathrm{d}z, \tag{5}$$

and ϵ is an effective emittance when looking at tangent pressure p.

The procedure starts by locating a point on the more opaque (narrow) CO_2 channel where $\epsilon_N \approx 1$, and deriving $\hat{T}_N$. Substituting $\hat{T}_N$ into equation (4) for the less opaque (wide) CO_2 channel leads to ϵ_W, from which a reference pressure p can be determined. The solution proceeds up the wide and narrow channels, using values of $\hat{T}$ in the hydrostatic equation to determine the pressure at the next level. In general, p_0 must be adjusted so that $\hat{T}_N \approx \hat{T}_W$.

When the profile $\hat{T}(p)$ is determined, equation (5) is inverted to yield the 'direct' solution, $T^{(1)}(p)$.

To complete the solution, (3) is written as

$$I(z_i) = W_{ij} B(z_j). \tag{6}$$

The $T^{(1)}(p)$ is used to calculate W_{ij}, equation (6) solved for $B^{(2)}$, and the solution iterated if desired. This allows improved vertical resolution, more complete allowance for temperature and pressure dependence, and the sounding of lower levels in the atmosphere.

The constituent retrieval proceeds similarly, except now we have

$$\epsilon_i = \epsilon_i(p, \hat{C}_i, \hat{T}),$$

where C is the concentration of the ith species. After ϵ_i is determined from (4), the distribution of $\hat{C}_i$ is obtained, and inverted to give the direct solution $C_i^{(1)}$. This is then used as the initial step in an equation of the form (6). In this case, improved solutions are obtained from the W_{ij} elements.

Inversion methods will be described in detail in future publications.

4. Results of limb profile inversion

(a) *L.r.i.r. results*

We first discuss the results of temperature retrieval, since this is the first step in any inversion. Figure 4 presents a temperature profile retrieved by using the initial inversion compared to a

nearby rocket measurement. There is quite reasonable agreement between these different observing techniques. We also see that the satellite retrieval does a good job of recovering fine scale structure.

There are two measures of quality to be applied to the retrievals; their repeatability (random error), and accuracy (systematic error). The former may be assessed by retrieving a sequence of radiance profiles in regions where the along-orbit gradient of atmosphere temperatures is small, a circumstance that can be checked. This is generally the case at low latitudes. Taking a series of observations, and assuming that the atmosphere is the same, the standard deviation of the temperatures at a level gives a measure of the end to end repeatability of the system of measurement plus inversion. This procedure returns values for the random error of less than 1 K from 50 to 5 mbar;† less than 2 K for 5–0.4 and < 2.5K at 0.25 mbar. The results then are very stable, and comparable to the repeatability of rocket measurements.

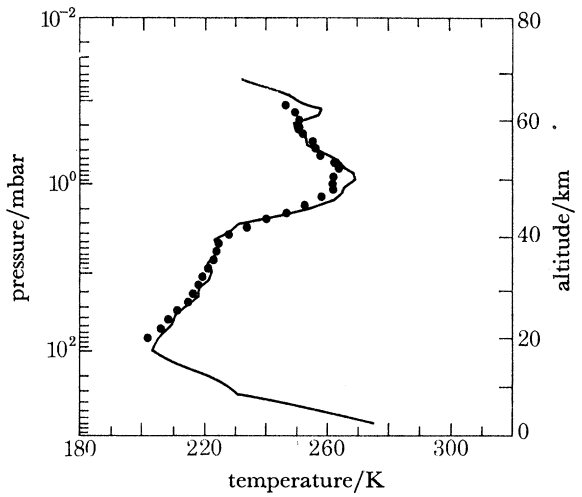

FIGURE 4. Temperature obtained from l.r.i.r. measurements, using the direct (first stage) inversion technique (points), compared to conventional rocketsonde and radiosonde measurements (solid line) at Wallops Island, Virginia (37.85° N, 75.48° W) at 1800 U.T. on 19 November 1975. The l.r.i.r. observations were obtained at 37.95° N, 73.60° W, at 1730 U.T.

The accuracy is much more difficult to assess with confidence, because of the lack of laboratory type standards for atmospheric measurements. Figure 5 presents a comparison for 47 cases using data from meteorological rockets – a familiar system which has been widely used. Comparisons include rocket results within 2° latitude and equivalent longitude, and 3 h time of l.r.i.r. results. The systematic differences are small; most are < 1°, and not statistically significant. These are themselves quite good, and certainly an excellent point from which to start the more detailed inversion.

The temperature profile from the data of figure 4, after the shell inversion, is shown in figure 6. The main differences are that it has somewhat finer vertical resolution, allows elimination of errors correlated with temperature, and, perhaps best, allows an extension to higher and especially to lower altitudes.

It should be pointed out that, aside from the use of four profiles to determine an instrumental parameter not well defined by laboratory measurements, there is no tuning of the transmittances or retrievel to give these results.

† 1 mbar = 10^2 Pa.

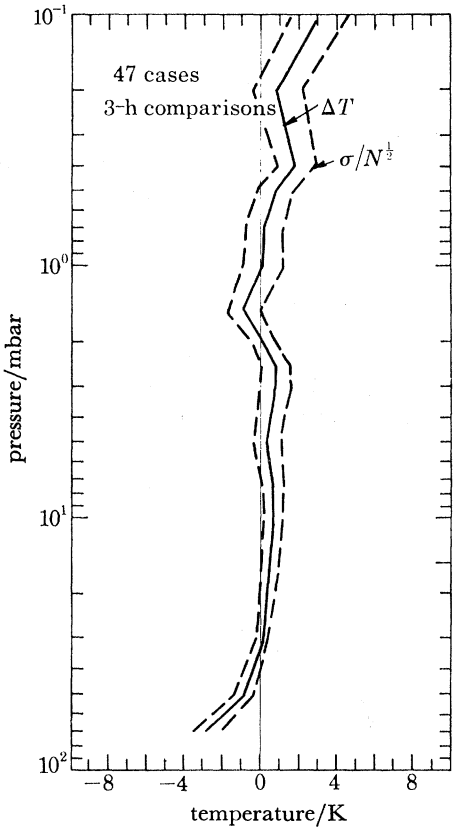

FIGURE 5. Comparison between l.r.i.r. and conventional rocketsondes and rawinsonde temperatures for 47 comparison cases (see text for criteria). Solid line displays l.r.i.r. minus conventional temperature. Broken lines bracket standard deviation of the mean difference.

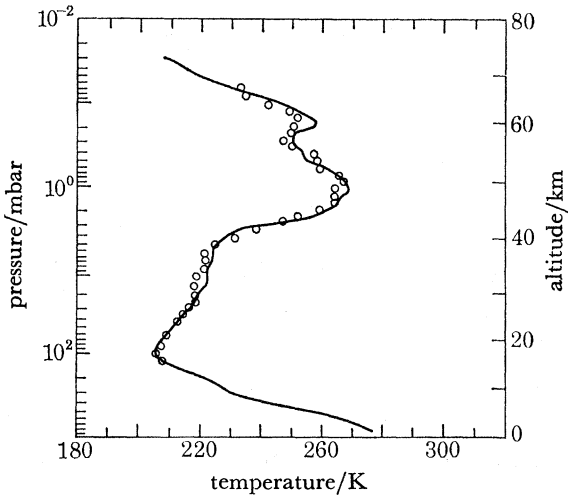

FIGURE 6. Temperature obtained from l.r.i.r. measurements, using a shell inversion to refine the first stage inversion (open circles), compared to conventional rocketsonde and radiosonde measurements (solid line). Conditions the same as in figure 4.

Figure 7 shows an l.r.i.r. ozone profile, compared to a rocket measurement by Krueger. The agreement is again good. Other noteworthy features are the resolution of the satellite retrieval, and its coverage, from 100 to 0.4 mbar, or the whole stratosphere and into the mesosphere.

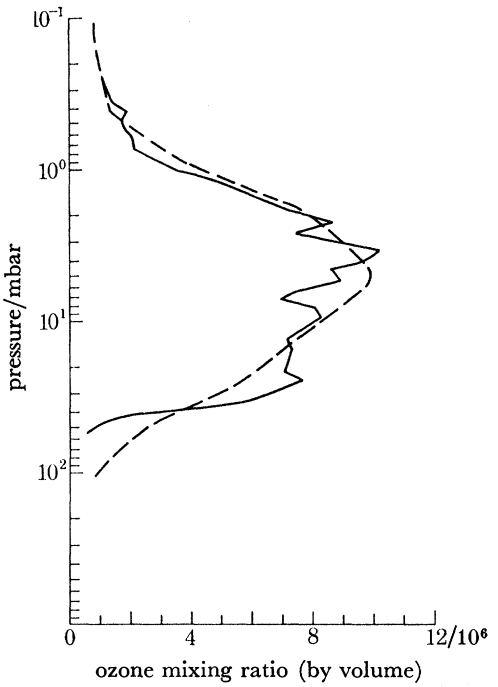

FIGURE 7. Comparison between l.r.i.r. ozone determination (dashes) and rocket ozone measurement using optical technique (solid line). Rocketsonde was obtained at Wallops Island at 1716 U.T. on 19 November 1975. The l.r.i.r. observations were obtained at 39.9° N, 75.0° W at 1730 U.T.

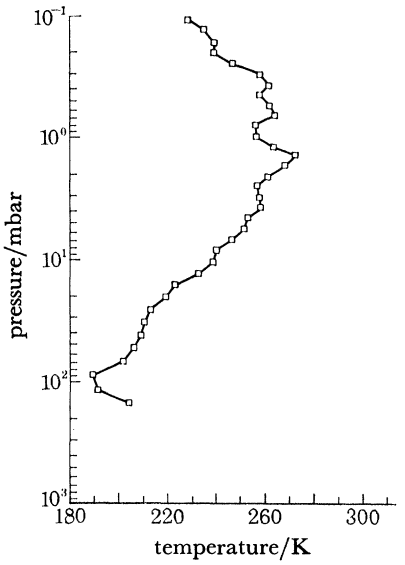

FIGURE 8. Preliminary l.i.m.s. temperature retrieval at the equator, 28 October 1978. The tropical tropopause region is clearly shown.

Again, the repeatability is less than 0.3 parts/10^6 by volume from 50 to 1 mbar, and less than 0.1 from 20 to 7 mbar, or 1 % at 10 mbar. The accuracy is difficult to assess, because of the fewer number of comparison cases and larger uncertainties of the ozone instruments, but the l.r.i.r. retrievals appear to be of comparable accuracy to the *in situ* devices.

The calibration of the H_2O channels has proved troublesome, and the signal:noise ratio is lower than expected. Results from this channel are not presented here.

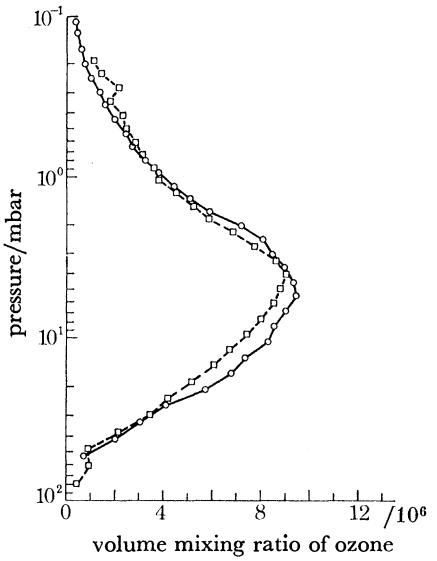

FIGURE 9. Preliminary l.i.m.s. ozone retrievals on 28 October 1978. Solid line, 109° E; dashed line, 111° W.

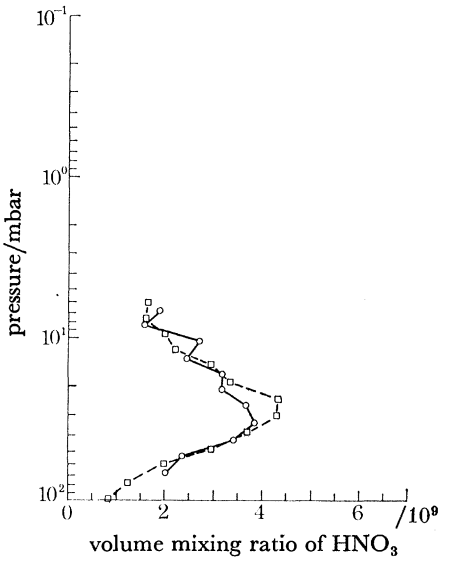

FIGURE 10. Preliminary l.i.m.s. nitric acid retrievals on 28 October 1978. Solid line, 109° E; dashed line, 111° W.

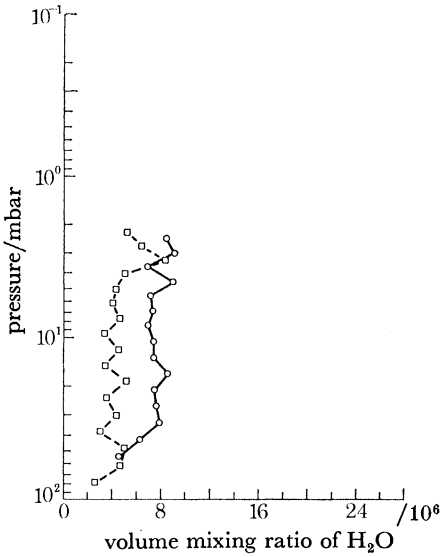

FIGURE 11. Preliminary l.i.m.s. water vapour retrievals on 28 October 1978. Solid line, 109° E; dashed line, 111° W.

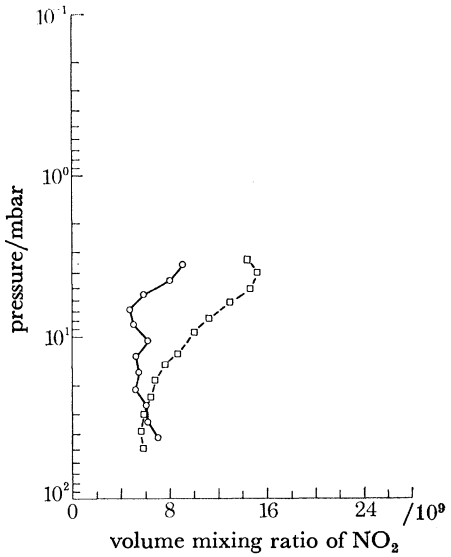

FIGURE 12. Preliminary l.i.m.s. nitrogen dioxide retrievals on 28 October 1978. Solid line, 109° E (day); dashed line, 111° W (night). A large diurnal variation is expected.

(*b*) *Preliminary l.i.m.s. results*

The l.i.m.s. results are very new at this time. All aspects of the instrument performance, atmospheric transmittances and retrieval techniques are not yet completely checked, and so the results presented here should be regarded as preliminary, but indicative.

An example of a l.i.m.s. temperature retrieval is shown in figure 8. Note that the tropical tropopause near 90 mbar is clearly seen, and the temperature retrieval extends into the upper tropopause. The lower altitude of the l.r.i.r. retrievals was limited not only by clouds, but also by the opacity of the CO_2 band itself. The l.i.m.s. channel 5 was spectrally broadened to facilitate retrieval into the upper tropopshere on cloud-free occasions.

Among the few profiles we have been able to look at to date, some go down to 240 mbar. L.i.m.s. temperature profiles, showing the lower stratosphere and tropopause region, will be supplied to the level II-*b* data sets of the global weather experiment (f.g.g.e.) to improve the depiction of the atmosphere for studies of weather forecasting.

L.i.m.s. ozone retrievals are presented in figure 9. The lower noise on l.i.m.s. allows retrievals to higher altitudes (and also lower, not shown). The results appear quite reasonable, although they have not yet been intercompared with other techniques.

Retrieved HNO_3 profiles are shown in figure 10. These are rather typical of values on this date, with peak values of 3–4 parts/10^9 by volume, peaking near 30 mbar. This appears to be typical of the Southern Hemisphere at this time. The HNO_3 profile at the equator appears to peak at higher altitude (*ca.* 10 mbar), with lower peak values (1–2 parts/10^9 by volume), with higher values at lower altitudes in the Northern Hemisphere. Initial comparison to *in situ* measurements shows reasonable agreement.

Two water vapour profiles at 30 S are presented in figure 11 (note the units are parts per million by volume: 1 part/10^6 by volume = 0.621 part/10^6 by mass). The mean concentrations are approximately 4 and 7 parts/10^6 by volume (2.5–4.4 parts/10^6 by mass) – within the range of accepted values. It is too early to say whether the indicated longitudinal variation is real or not.

Finally, two NO_2 retrievals are shown in figure 12. The daytime values are slightly lower at latitudes other than $\pm 60°$, night-time values higher. All profiles show the expected night-time increase of NO_2, by about a factor of two. Because of uncertainties in the basic spectroscopic parameters, these results are more provisional than the other l.i.m.s. results.

Note that for HNO_3, H_2O and NO_2, results are presented only to about 5 mbar because final transmittance values are not yet available. Retrievals to about 1 mbar should be possible for all these species.

5. Application of l.r.i.r. results

Observations of the type presented above allow the stratosphere to be observed globally with a detail not previously possible. We shall mention just a few of the possible uses of such data.

(*a*) *Mesospheric ozone distribution*

Riegler *et al.* (1976, 1977) have derived the night-time ozone distributions down to *ca.* 45 km from measurements of the occultation of β-Centauri obtained from the Copernicus telescope on the OAO-3 satellite. Night-time concentrations derived from l.r.i.r. measurements up to 55 km for the previous day, at the same latitude and bracketing longitudes, are a factor of 3

smaller than the Copernicus results, and in much better agreement with measurements by other techniques and theoretical models. Contrary to the Copernicus results, they indicate that photochemical theory can explain the ozone concentration in the lower mesosphere reasonably well.

(*b*) *Diurnal variation of ozone*

A Sun-synchronous orbit is not a good one for the study of diurnal changes, since a given latitude is viewed at the same two local times every day. One can measure day–night differences, however. For the l.r.i.r. scan track, there are latitudes at which a location will be observed on the day side of the Earth, and several orbits later will be observed again on the night side. In this few hours interval, and at high enough altitudes, one would expect the effects of transports to be minimal and the differences in ozone concentration to be due to photochemical effects. Preliminary results show night-time values exceeding day-time values by up to 20 % ($\pm$ 10 %) in the layer from 0.4 to 0.07 mbar (56–66 km), decreasing to no detectable change at 1 mbar. These studies will be amplified and extended in the future.

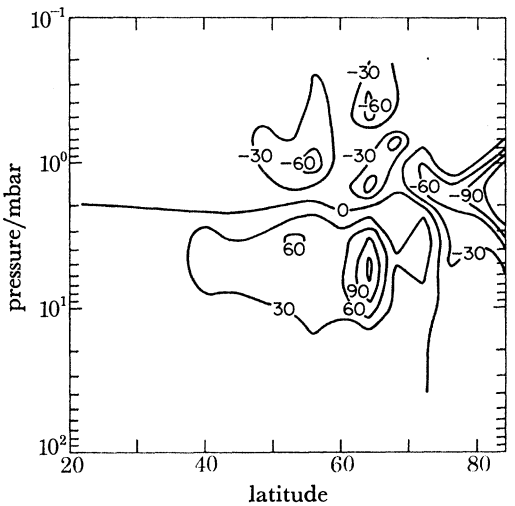

FIGURE 13. Ozone transports due to geostrophic eddies. Units are parts/10^6 (by volume) m s^{-1}.

(*c*) *Transports*

Because temperature is measured as well as constituent concentrations, geopotential heights and geostrophic winds may be derived, and transports by geostrophic eddies directly calculated. The key to this procedure is the method of analysing the spatial variation of the fields. We have used the approach suggested by Rodgers (1976), in which the observations are Kalman filtered to update the Fourier coefficient representation of the fields on a latitude circle. Analyses are produced at each 4° of latitude for T, O_3, and $\Delta\phi_{30}$, the thickness above the 30 mbar surface, at 17 pressure levels. The geopotential height is obtained by adding the thickness to the conventionally analysed geopotential at 30 mbar, to give a result of the form

$$\phi(p,\theta,t) = \phi_0(p,\theta,t) + \sum_{n=1}^{6} a_n(p,\theta,t)\sin\frac{2\pi n\lambda}{360} + \sum_{n=1}^{6} b_n(p,\theta,t)\cos\frac{2\pi n\lambda}{360},$$

where p is the pressure, θ the latitude, t the time and λ is the longitude. Calculation of the geostrophic wind, and especially of the meridional wind associated with the eddies ($v' \propto \partial\phi/\partial\lambda$)

follows immediately. Finally, when the ozone concentration is similarly expressed, the transports by wavenumber n, $\overline{v'_n O'_{3n}}$, may be immediately obtained. A cross section of eddy transports of ozone on a single day is shown in figure 13. Of course, this is only part of the transport, since there are also compensating mean meridional transports, as well as photochemical effects. With observations as detailed as these, it should be possible to derive the meridional circulation (as Hartmann (1976) did), to obtain a complete picture of the transport.

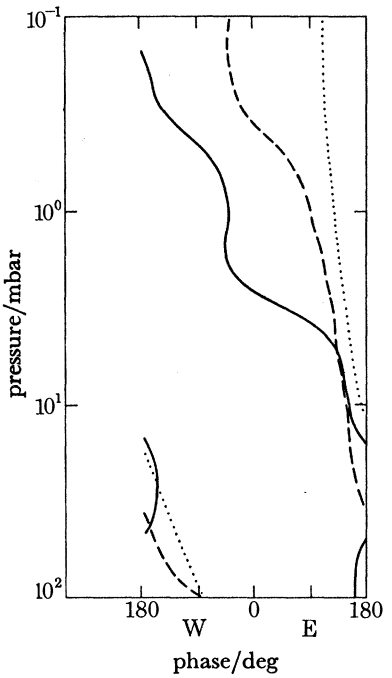

FIGURE 14. Phases of wave in temperature (dashed line), ozone mixing ratio (solid line) and geopotential height (dotted line) as a function of altitude on 1 November 1975. The in-phase relation between ozone mixing ratio and geopotential indicates dynamical control, while an exactly out of phase relation between ozone and temperature signifies photochemical control (Hartmann & Garcia (1979)).

(*d*) *Photochemistry*

Finally, these data provide information on the basic ozone photochemistry. The phase of the wavenumber 1 ($n = 1$) variation of ozone mixing ratio (μ_3), temperature and geopotential are shown for 60° N on 1 November 1975 in figure 14. Hartmann & Garcia (1979) have used a simple mechanistic model to show that when the ozone distribution is dynamically controlled, the ozone mixing ratio will be in phase with the geopotential, whereas under photochemical control it will be 180° out of phase with the temperature. This latter results from temperature dependence of the reaction rates, experimentally observed in the atmosphere by Barnett *et al.* (1975). The data shown in figure 14 thus indicate dynamical control of the ozone distribution up to 5 mbar (*ca.* 35 km), with photochemical control above 2 mbar (*ca.* 45 km). This directly confirms the behaviour predicted on the basis of the photochemical models, and the existence of the two régimes (with an interesting transition region between).

6. Conclusions

The results presented here demonstrate the ability of limb scanning radiometers to provide temperature and ozone profiles with high vertical resolution from the troposphere into the lower mesosphere that are very repeatable and agree well with rocket measurements. They also show for the first time the ability to measure constituents in the parts/10^9 range (HNO_3, NO_2) from a satellite. Work is still required to establish the accuracy of the new measurements.

Finally, the preliminary scientific results give a glimpse of the power and utility of these data in the solution of problems in the middle atmosphere.

We gratefully acknowledge the contributions of G. P. Anderson, R. Garcia, W. Kohri, S. Nolte and V. Rinehart, all of N.C.A.R., to the work presented here. This activity was partially supported by the National Aeronautics and Space Administration through Contract S40135 G and Order Number L36446 A. The National Center for Atmospheric Research is sponsored by the National Science Foundation.

References (Gille *et al.*)

Bailey, P. L. & Gille, J. C. 1978 In *Remote sensing of the atmosphere: inversion methods and applications* (ed. A. L. Fymat & V. E. Zuev), pp. 115–122. Amsterdam: Elsevier.

Barnett, J. J., Houghton, J. T. & Pyle, J. A. 1975 *Q. Jl R. met. Soc.* **101**, 245–257.

Gille, J. C., Bailey, P., House, F. B., Craig, R. A. & Thomas, J. R. 1975 In *The Nimbus* 6 *user's Guide* (ed. J. E. Sissala). Greenbelt, Maryland: National Aeronautics and Space Administration.

Gille, J. C. & House, F. B. 1971 *J. atmos. Sci.* **28**, 1427–1442.

Gille, J. C. & Bailey, P. L. 1978 In *Remote sensing of the atmosphere: inversion methods and applications* (ed. A. L. Fymat & V. E. Zuev), pp. 107–113. Amsterdam: Elsevier.

Hartmann, D. L. 1976 *J. atmos. Sci.* **33**, 1789–1802.

Hartmann, D. L. & Garcia, R. R. 1979 *J. atmos. Sci.* **36**, 350–364.

Riegler, G. R., Drake, J. F., Liu, S. C. & Cicerone, R. J. 1976 *J. geophys. Res.* **81**, 4997–5001.

Riegler, G. R., Atreya, S. K., Donaheu, T. M., Liu, S. C. & Wasser, B. 1977 *Geophys. Res. Lett.* **4**, 145–148.

Rodgers, C. D. 1976 In *Inversion methods in atmospheric remote sounding* (ed. A. Deepak), pp. 117–138. New York: Academic Press.

Russell, J. M. III & Gille, J. C. 1978 In *The Nimbus* 7 *user's Guide* (ed. C. R. Madrid), pp. 71–103. Greenbelt Maryland: National Aeronautics and Space Administration.

PHILOSOPHICAL TRANSACTIONS OF THE ROYAL SOCIETY A MATHEMATICAL, PHYSICAL & ENGINEERING SCIENCES